Scientific and Social Research, 2026, Volume 8, Issue 10
https://bbwpublisher.com/journal/SSR
Online ISSN: 2981-9946
Print ISSN: 2661-4332

Variable-Property Coupled Heat and Moisture Transfer During Hot-Air Drying of Chinese Medicinal Materials

Yiming Hao*, Jiashu Hu, Luntao Hu

School of Technology, Beijing Forestry University, Beijing 100083, China

***Corresponding author:** Yiming Hao, hao_5882@163.com

Copyright: © 2026 Author(s). This is an open-access article distributed under the terms of the Creative Commons Attribution License (CC BY 4.0), permitting distribution and reproduction in any medium, provided the original work is cited.

Abstract: A one-dimensional axisymmetric heat and moisture transfer model is developed for hot-air drying of Chinese medicinal materials under time-varying boundaries, state-dependent properties, and radial shrinkage. A material reference domain derived from observed radii and uniform proportional shrinkage uses a domain-wide moisture constraint to locate the endpoint. At 3 h, the center-to-surface temperature difference is 0.1172 °C, while center and surface moisture contents are 1.7662 and 1.0081 kg/kg. Fixed-size and shrinking cases reach the endpoint at 57.4743 and 51.0885 h. Three-grid calculations give GCI < 0.001% for 3201 nodes; an FVM cross-check gives 8.18–11.62-fold speedup. Local sensitivity is dominated by the equivalent convective mass-transfer coefficient.

Keywords: Chinese medicinal materials; Heat and moisture transfer; State-dependent properties; Radial shrinkage; Numerical verification; Drying endpoint

Online publication: November 25, 2026

1. Introduction

Hot-air drying is widely used in the primary processing of Chinese medicinal materials, yet temperature and moisture evolve nonuniformly because external conditions, geometry, and internal state change together. Distributed heat-and-moisture models have progressively incorporated non-isothermal transport, variable properties, and shrinkage [1–6]. Data-driven numerical drying approaches have also been explored [7].

Complex multiphysics descriptions require parameters and structural data that are often unavailable. This work therefore develops a one-dimensional axisymmetric model with PCHIP environmental boundaries, state-dependent properties, a radial-shrinkage reference domain, and a domain-wide endpoint. It evaluates thermal and moisture time scales, center drying lag, endpoint differences, numerical consistency, FVM speedup, and local surface-transfer sensitivity.

2. Nonlinear coupled heat and moisture transfer model

2.1. Physical domain and basic assumptions

The material is treated as a cylindrical, continuous, homogeneous, isotropic body with one-dimensional radial transport. Heat transfer is conductive, moisture transport is by effective diffusion, and the surface exchanges heat and moisture convectively [3, 5–6, 8–9]. Radiation, reaction heat, explicitly resolved latent heat, multiphase equilibrium, and phase-change coupling are not included.

2.2. Initial conditions and time-dependent boundaries

Temperature and dry-basis moisture content are initially uniform. The center has zero flux; third-kind heat and equivalent mass-transfer conditions apply at the surface. Discrete environmental temperature and humidity are interpolated with PCHIP, with temperature converted to the absolute scale once. The observation nodes are retained.

$$T_K(r,0) = T_0 = 301.15K \tag{1}$$

$$C(r,0) = C_0 = 2.55kg/kg \tag{2}$$

$$\left.\frac{\partial T_K}{\partial r}\right|_{r=0} = 0, \left.\frac{\partial C}{\partial r}\right|_{r=0} = 0 \tag{3}$$

$$-k(C)\left.\frac{\partial T_K}{\partial r}\right|_{r=R_0} = h\left[T_s(t) - T_{\infty,K}(t)\right] \tag{4}$$

$$-D(C,T_K)\left.\frac{\partial C}{\partial r}\right|_{r=R_0} = h_m\left[C_s(t) - C_e(t)\right]$$

$$T_\infty(t) = P_T(t) \tag{5}$$

$$C_e(t) = P_C(t) \tag{6}$$

2.3. Heat and moisture governing equations

The fixed-size model uses a sensible-heat balance and effective Fickian moisture diffusion. State-dependent properties remain inside the flux operators, so coupling is introduced through the local thermo-hygroscopic state.

$$\rho(C)c_p(C)\frac{\partial T_K}{\partial t} = \frac{1}{r}\frac{\partial}{\partial r}\left(rk(C)\frac{\partial T_K}{\partial r}\right), \quad 0 < r < R_0 \tag{7}$$

$$\frac{\partial C}{\partial t} = \frac{1}{r}\frac{\partial}{\partial r}\left(rD(C,T_K)\frac{\partial C}{\partial r}\right), \quad 0 < r < R_0 \tag{8}$$

2.4. State-dependent variable properties and coupling relations

The relations for $\rho(C)$, $c_p(C)$, $k(C)$, and $D(C,T)$ are retained. Moisture changes heat storage and conduction, while temperature and moisture jointly control diffusivity, forming state-feedback coupling.

$$\rho(C) = 650 + 128C \tag{9}$$

$$c_p(C) = 1450 + \frac{2736C}{C+1} \tag{10}$$

$$k(C) = 0.21 + \frac{0.38C}{C+1} \tag{11}$$

$$A(C) = \rho(C)c_p(C) \tag{12}$$

$$D(C, T_K) = 2.4 \times 10^{-3} exp\left(-\frac{0.45}{C}\right) exp\left(-\frac{3850}{T_K}\right) \tag{13}$$

3. Simplified fixed-domain numerical framework for radial shrinkage

3.1. Time-dependent environmental boundary for long-term drying

Beyond the observation interval, the final observed environmental state is held constant for numerical continuation only; it is not a prediction of future drying-room conditions.

$$C_e(t) = \begin{cases} P_C(t), & 0 \le t \le t_e, \\ C_e^{60}, & t > t_e. \end{cases} \tag{14}$$

3.2. Construction of the dynamic radius function

The radius is obtained directly from observations using PCHIP and terminal-value extension. No independent shrinkage constitutive law is introduced.

$$\{(t_i, R_i)\}_{i=1}^{N_R} \tag{15}$$

$$R(t) = \begin{cases} P_R(t), & 0 \le t \le t_R, \\ R(t_R), & t > t_R. \end{cases} \tag{16}$$

3.3. Simplified material reference-domain model based on uniform proportional shrinkage

Uniform proportional radial shrinkage defines ξ=r/R(t) and maps the material to a fixed reference domain. The internal operators contain $R^{-2,}$ and the surface boundary contains R^{-1}. Moving-boundary, ALE, and shrinkage treatments provide related alternatives [1, 10–15]. This formulation is a material-reference closure rather than a direct Eulerian coordinate transformation; therefore, no explicit R'(t) drift term is introduced under the stated assumptions. The shrinking case retains its stated property relations and is applicable only within this closure.

$$\xi = \frac{r}{R(t)}, \quad 0 \le \xi \le 1 \tag{17}$$

$$\rho_s(C) = 760 + 90C \tag{18}$$

$$c_{p,s}\left(C\right)=1850+2150\frac{C}{C+1} \tag{19}$$

$$k_s\left(C\right)=0.12+0.20\frac{C}{C+1} \tag{20}$$

$$D_s\left(C,T_K\right)=4.2\times10^{-4}exp\left(-0.30C\right)exp\left(-\frac{3850}{T_K}\right) \tag{21}$$

$$\rho_s\left(C\right)c_{p,s}\left(C\right)\frac{\partial T_K}{\partial t}=\frac{1}{R^2\left(t\right)}\frac{1}{\xi}\frac{\partial}{\partial\xi}\left(\xi k_s\left(C\right)\frac{\partial T_K}{\partial\xi}\right) \tag{22}$$

$$0<\xi<1 \tag{23}$$

$$\frac{\partial C}{\partial t}=\frac{1}{R^2\left(t\right)}\frac{1}{\xi}\frac{\partial}{\partial\xi}\left(\xi D_s\left(C,T_K\right)\frac{\partial C}{\partial\xi}\right) \tag{24}$$

$$\left.\frac{\partial T_K}{\partial\xi}\right|_{\xi=0}=0,\left.\frac{\partial C}{\partial\xi}\right|_{\xi=0}=0 \tag{25}$$

$$\begin{aligned}-\frac{k_s\left(C\right)}{R\left(t\right)}\left.\frac{\partial T_K}{\partial\xi}\right|_{\xi=1}&=h\left[T_s\left(t\right)-T_{\infty,K}\left(t\right)\right]\\-\frac{D_s\left(C,T_K\right)}{R\left(t\right)}\left.\frac{\partial C}{\partial\xi}\right|_{\xi=1}&=h_m\left[C_s\left(t\right)-C_e\left(t\right)\right]\end{aligned} \tag{26}$$

3.4. Drying endpoint determination based on a domain-wide state constraint

The maximum moisture content $C_{max}(t)$ is compared with the limiting value C_{lim}. The endpoint t_d is the first downward zero of the event function $C_{max}(t)-C_{lim}$; the next 60 s storage node confirms that the domain is below the threshold.

$$C_{\max}\left(t\right)=\max_{0\le\xi\le1}C\left(\xi,t\right) \tag{27}$$

$$t_d=\inf\{t>0:C_{\max}\left(t\right)\le C_{\lim}\} \tag{28}$$

$$g\left(t\right)=C_{\max}\left(t\right)-C_{\lim} \tag{29}$$

3.5. Numerical solution method

MATLAB R2025a pdepe with m=1 solves the fixed physical domain and the shrinking reference domain. A 401-node calculation prelocalizes the endpoint; the formal 3201-node solution uses RelTol=10^{-8}, AbsTol=10^{-10}, MaxStep=60 s, event detection, and physical/reference-domain mapping. Output intervals are used only for storage; internal integration remains adaptive. The two-stage procedure is retained for endpoint prelocalization, not acceleration.

$$g(t) = C_{\max}(t) - C_{lim} \tag{30}$$

$$\xi_j(t) = \frac{r_j}{R(t)} \tag{31}$$

4. Results and discussion

4.1. Transient evolution of the temperature and moisture fields

Temperature equilibrated substantially faster than moisture. The center-to-surface temperature difference decreased from 3.2236℃ at 0.5 h to 0.1172℃ at 3 h, whereas the corresponding moisture difference remained 0.7581 kg/kg. F**igure 1** shows the radial and temporal evolution, confirming persistent moisture nonuniformity after the temperature field had nearly equilibrated.

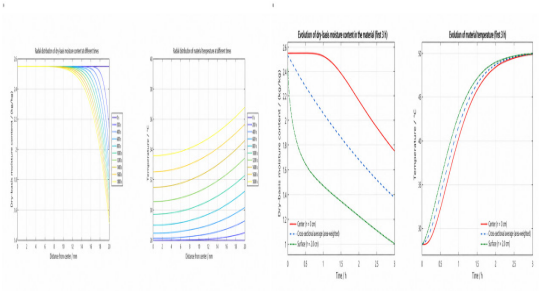

Figure 1. Radial and temporal evolution of dry-basis moisture content and temperature during the first 3 h

4.2. Radial moisture gradients and center drying lag

During long-term fixed-size drying, the center remained the wettest location. At 48 h, the center and surface moisture contents were 0.1618 and 0.0537 kg/kg, respectively; the center reached the limiting value of 0.1500 kg/kg at 57.4743 h and therefore controlled the overall endpoint. **Figure 2** illustrates the evolution of the domain-wide maximum moisture content and the threshold interface.

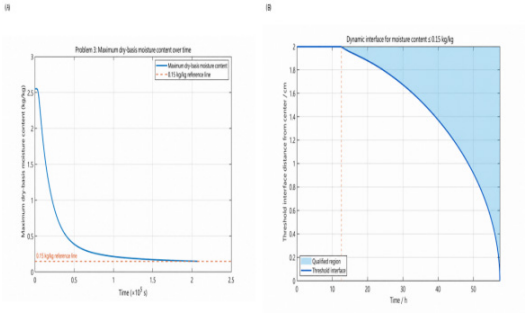

Figure 2. (A) Domain-wide maximum moisture content and threshold; (B) threshold-interface distance to the center

4.3. Predicted evolution under radial shrinkage

Under radial shrinkage, the radius decreased from 2.0 cm to 1.2000 cm at the predicted endpoint of 51.0885 h. At that time, the center and surface moisture contents were 0.1500 and 0.0526 kg/kg. The normalized

coordinate ξ therefore provides a consistent description as fixed physical locations leave the shrinking material domain. **Figure 3** shows the corresponding moisture evolution in the material reference domain.

The fixed-size and shrinkage cases use different state-dependent property relations; their endpoint difference should therefore not be interpreted as the isolated effect of geometric shrinkage.

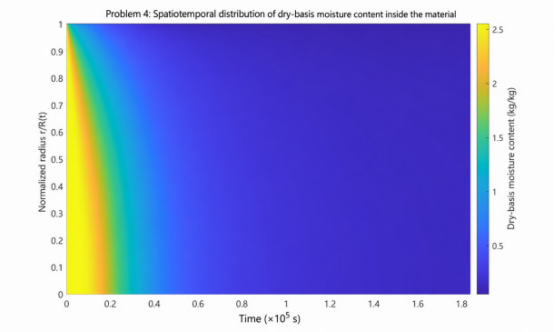

Figure 3. Spatiotemporal moisture evolution in the normalized material reference domain

4.4. Drying endpoint and spatial differences

The endpoint results are summarized in **Table 1**. Both cases are center-controlled, while the shrinkage case retains a center-to-surface difference of 0.0974 kg/kg at the endpoint. Thus, satisfying the domain-wide criterion does not imply spatially uniform moisture, but only that the wettest location has reached the prescribed limit.

Table 1. Predicted drying endpoints

Case	t_d / h	R_d / cm	C_{center} / kg kg^{-1}	$C_{surface}$ / kg kg^{-1}
Fixed-size	57.4743	2.0000	0.1500	0.0526
Radial shrinkage	51.0885	1.2000	0.1500	0.0526

4.5. Numerical consistency and convergence tests

Numerical verification included integral consistency, three-grid refinement, time-integration perturbation, and a separate FVM spatial-discretization cross-check. For the fixed-size case, the temperature and moisture integral residuals were 3.617×10^{-7} and 4.072×10^{-7}; the corresponding 95th-percentile values for the shrinking case were 1.948×10^{-2} and 5.487×10^{-5}. Three-grid calculations yielded observed orders of 1.9258 and 2.0990 with $R_{asym}\approx1$, while the GCI of the 3201-node grid remained below 0.001% (**Table 2**), indicating adequate spatial resolution following the standard GCI procedure [16].

Relative to the strict integration settings, the baseline endpoints changed by only 0.010988 and 0.015310 s, with maximum field differences of 1.7×10^{-5} °C and 9.30×10^{-8} kg/kg. The FVM cross-check produced $\Delta T_{max}=1.5\times10^{-5}$ °C and $\Delta C_{max}=6.94\times10^{-8}$ kg/kg over the first 3 h and provided 8.18–11.62-fold speedup. The two-stage endpoint search reproduced the same endpoints but did not reduce runtime.

Table 2. Summary of numerical verification

Verification	Fixed-size	Radial shrinkage
Observed order p	1.9258	2.0990
GCI of 3201-node grid / %	0.000676	0.000069
R_{asym}	0.999996	1.000000
FVM endpoint difference / %	0.0031	6.0×10^{-7}
FVM speedup	8.18×	11.62×

$$p = \frac{\ln\left|\frac{\phi_3 - \phi_2}{\phi_2 - \phi_1}\right|}{\ln r} \tag{32}$$

$$GCI_{12} = F_s \frac{\left|(\phi_1 - \phi_2)/\phi_1\right|}{r^p - 1} \times 100\%, \tag{33}$$

$$S_{FVM} = \frac{t_{pdepe}}{t_{FVM}}. \tag{34}$$

4.6. Parameter sensitivity and sources of uncertainty

Within the ±20% perturbation range, $h_m$changed the 3-h average moisture content by 0.2333 kg/kg and the fixed-size endpoint by 2.729 h, whereas h produced changes of only 0.0083 kg/kg and approximately 117.9 s, respectively. This stronger response arises because $h_m$directly controls the surface moisture flux, while h affects moisture transport indirectly through the temperature-dependent properties. The analysis is local and does not constitute a global sensitivity ranking.

5. Model strengths and limitations

5.1. Model strengths

The one-dimensional formulation preserves radial nonuniformity while using observable boundaries. Its material reference domain handles uniform shrinkage, and C_{max}(t) gives a conservative endpoint governed by the slowest-drying location. Grid and FVM checks support numerical consistency.

5.2. Model limitations

The model assumes a homogeneous, isotropic, one-dimensional medium and uniform proportional shrinkage. It omits explicit latent heat and multiphase coupling, relies on empirical properties and transfer coefficients, and lacks independent experimental validation [15, 17]. Long-term boundary and radius extensions add uncertainty. Independent drying experiments are therefore required for physical validation and parameter calibration.

6. Conclusions

A one-dimensional axisymmetric variable-property model with time-varying boundaries and a material reference domain was developed for hot-air drying of Chinese medicinal materials. Temperature equilibrated

faster than moisture: at 3 h, the temperature difference was 0.1172 °C, while center and surface moisture contents were 1.7662 and 1.0081 kg/kg. Fixed-size and radial-shrinkage endpoints were 57.4743 and 51.0885 h. Three-grid convergence and FVM cross-checking confirmed numerical consistency, while local sensitivity was dominated by the mass-transfer coefficient; independent experiments remain necessary for validation.

Disclosure statement

The authors declare no conflict of interest.

References

[1] Adrover A, Brasiello A, Ponso G, 2019, A Moving Boundary Model for Food Isothermal Drying and Shrinkage: General Setting. Journal of Food Engineering, 2019(244): 178–191. https://doi.org/10.1016/j.jfoodeng.2018.09.018

[2] Arpaci E, Atayılmaz ŞÖ, Gemici Z, 2025, Exploring Mathematical Modeling and CFD in Convective Drying of Fruits and Vegetables: A Review. Food and Bioprocess Technology, 18(4): 3195–3222. https://doi.org/10.1007/s11947-024-03627-2

[3] Hernández-Flores OA, Callejas-Pérez LA, Romero-Salazar C, et al., 2026, Numerical Analysis of Convective Drying with Pulsed Airflow. Journal of Food Process Engineering, 49(5): e70518. https://doi.org/10.1111/jfpe.70518

[4] Wang L, Li C, Liu M, et al., 2024, Research Status of Drying Technology and Equipment for Chinese Medicinal Materials. Transactions of the Chinese Society of Agricultural Engineering, 40(2): 1–28. https://doi.org/10.11975/j.issn.1002-6819.202306104

[5] Chen P, Chen N, Zhu W, et al., 2023, A Heat and Mass Transfer Model of Peanut Convective Drying Based on a Two-Component Structure. Foods, 12(9): 1823. https://doi.org/10.3390/foods12091823

[6] Tzempelikos DA, Mitrakos D, Vouros AP, et al., 2015, Numerical Modeling of Heat and Mass Transfer during Convective Drying of Cylindrical Quince Slices. Journal of Food Engineering, 2015(156): 10–21. https://doi.org/10.1016/j.jfoodeng.2015.01.017

[7] Malekjani N, Bück A, Kharaghani A, et al., 2026, SDD-PINN: Physics-informed Neural Network for Single Droplet Drying. Digital Chemical Engineering, 2026(19): 100306. https://doi.org/10.1016/j.dche.2026.100306

[8] Costa de Sousa R, Binda Silva Costa A, Martins Freitas MD, et al., 2024, Convective Drying of Black Pepper: Experimental Measurements and Mathematical Modeling. Food and Bioproducts Processing, 2024(143): 102–116. https://doi.org/10.1016/j.fbp.2023.10.009

[9] Pereira da Silva W, Silva CMDPS, Gama FJA, 2014, Estimation of Thermo-Physical Properties of Products with Cylindrical Shape during Drying. Journal of Food Engineering, 2014(141): 65–73. https://doi.org/10.1016/j.jfoodeng.2014.05.010

[10] Martínez Vera C, Vizcarra Mendoza MG, 2022, Concentration-dependent Moisture Diffusion Coefficient Estimation in Peas Drying Considering Shrinkage. Biosystems Engineering, 2022(218): 256–273. https://doi.org/10.1016/j.biosystemseng.2022.04.016

[11] Das R, Islam M, Saini P, et al., 2025, Finite Element Modeling of Banana Slices in Convective Drying using an ALE Approach. Thermochimica Acta, 2025(749): 180024. https://doi.org/10.1016/j.tca.2025.180024

[12] Li J, Huang Y, Gao M, et al., 2024, Shrinkage Properties of Porous Materials during Drying: A Review. Frontiers in Materials, 2024(11): 1330599. https://doi.org/10.3389/fmats.2024.1330599

[13] Li Y, Liang M, Li J, et al., 2025, Simulation and Experimental Studies of Heat-Mass Transfer and Stress–Strain in Carrots During Hot Air Drying. Agriculture, 15(5): 484. https://doi.org/10.3390/agriculture15050484

[14] Sinha A, Bhargav A, 2022, A Simplified Modelling Approach for Predicting Shrinkage and Sensitive Material Properties during Low Temperature Air Drying. Journal of Food Engineering, 2022(317): 110732. https://doi.org/10.1016/j.jfoodeng.2021.110732

[15] Zhu Y, Wang P, Sun D, et al., 2021, Multiphase Porous Media Model with Thermo-Hydro and Mechanical Bidirectional Coupling for Food Convective Drying. International Journal of Heat and Mass Transfer, 2021(175): 121356. https://doi.org/10.1016/j.ijheatmasstransfer.2021.121356

[16] Celik IB, Ghia U, Roache PJ, et al., 2008, Procedure for Estimation and Reporting of Uncertainty Due to Discretization in CFD Applications. Journal of Fluids Engineering, 130(7): 078001. https://doi.org/10.1115/1.2960953

[17] Purlis E, 2019, Modelling Convective Drying of Foods: A Multiphase Porous Media Model Considering Heat of Sorption. Journal of Food Engineering, 2019(263): 132–146. https://doi.org/10.1016/j.jfoodeng.2019.05.028

Publisher's note

Bio-Byword Scientific Publishing remains neutral with regard to jurisdictional claims in published maps and institutional affiliations.